Tracklet Association by Online Target-Specific Metric Learning and Coherent Dynamics Estimation

Bing Wang, *Student Member, IEEE*, Gang Wang, *Member, IEEE*, Kap Luk Chan, *Member, IEEE*, and Li Wang, *Member, IEEE*

Abstract—In this paper, we present a novel method based on online target-specific metric learning and coherent dynamics estimation for tracklet (track fragment) association by network flow optimization in long-term multi-person tracking. Our proposed framework aims to exploit appearance and motion cues to prevent identity switches during tracking and to recover missed detections. Furthermore, target-specific metrics (appearance cue) and motion dynamics (motion cue) are proposed to be learned and estimated online, i.e., during the tracking process. Our approach is effective even when such cues fail to identify or follow the target due to occlusions or object-to-object interactions. We also propose to learn the weights of these two tracking cues to handle the difficult situations, such as severe occlusions and object-to-object interactions effectively. Our method has been validated on several public datasets and the experimental results show that it outperforms several state-of-the-art tracking methods.

Index Terms—Multi-object tracking, tracklet association, target-specific metric learning, motion dynamics, network flow optimization

1 Introduction

In this paper, we address the challenges in long-term tracking of multiple persons in a complex scene captured by a single, uncalibrated camera with an aim of achieving consistent person identity tracking (i.e., no identity switches). This is a challenging problem due to many sources of uncertainty, such as clutter, serious occlusions, targets interactions, and camera motion.

Recently, significant progress has been reported in human detection [1], [2], [3], [4], [5], [6], [7], and this promotes the popular tracking paradigm: detect-then-track [8], [9], [10], [11], [12], [13], [14], [15], [16]. The main idea is that a human detector is run on each frame to detect targets of interest, and then detection responses are linked across multi-frames to obtain target trajectories. In [11], [12], [13], [16], the authors formulate the multi-target data association as a network flow optimization problem. Zhang et al. [11] use a push-relabel method [17] to solve the min-cost flow problem. Berclaz et al. [12] and Pirsiavash et al. [13] propose to use successive shortest path algorithms, which can achieve roughly the same tracking results with less computation cost. In a more recent paper, Butt et al. [16] incorporate higher-order track smoothness constraints, such as constant velocity, for multi-target tracking. However, due to the limitation of the appearance cues used for tracking, the methods mentioned above usually cannot deal with longer term tracking to obtain a complete trajectory of a target. This is because prolonged occlusions and target-to-target interactions will result in fragmentation of a trajectory.

By using of the information from previous, current, and subsequent frames, trajectory can be recovered from the fragments and tracking errors such as missed tracks or identity switches can be corrected. In our earlier work [18], we advocate a discriminative target-specific appearance-based affinity model to reinforce the appearance cues for multi-person tracking. Unlike the PIRMPT system proposed by [19], which requires off-line learned local descriptors, our target-specific metrics are online learned during tracking. In [18], we utilized a motion constraint based on heuristics. In this paper, we exploit motion dynamics to further improve tracking of target's identity. Furthermore, we study the significance of the appearance and motion cues on tracking performance independently. Different from previous works [19], [20], [21], which simply multiply the motion and appearance affinities to obtain the linking probabilities of two tracklets, we separately develop a learning algorithm to automatically learn the weights of the two terms from labeled training data. The learned weights can enhance the tracking cues with strong discriminative power and suppress the tracking cues with weak discriminative power. As a result, the weighted tracking cues can disambiguate the targets' respective identities better even in situations such as the one depicted in Fig. 1.

A typical way of implementing the popular "detect-then-track" paradigm is to track multiple targets frame by frame, which often encounters irrecoverable errors if a target is undetected in one or more successive frames or if two detections are erroneously linked. To overcome this weakness, global trajectory optimization over batches of frames have been proposed in recent years, using methods such as Linear Programming [22], [23] and Dynamic Programming [13], [24]. These

• *The authors are with the School of Electrical and Electronic Engineering, Nanyang Technological University, 50 Nanyang Avenue, Singapore, 639798. E-mail: {wang0775, wanggang, eklchan, wa0002li}@ntu.edu.sg.*

Manuscript received 14 Dec. 2014; revised 26 Mar. 2016; accepted 1 Apr. 2016. Date of publication 5 Apr. 2016; date of current version 13 Feb. 2017. Recommended for acceptance by D. Forsyth.
For information on obtaining reprints of this article, please send e-mail to: reprints@ieee.org, and reference the Digital Object Identifier below.
Digital Object Identifier no. 10.1109/TPAMI.2016.2551245

Fig. 1. A difficult scenario of high appearance similarity among targets. (Frames from PETS dataset with pedestrian identities labeled by our method): Despite individuals 1 and 8 dressed in similarly colored clothes and severe occlusions and interactions between individuals 1, 8, and 9, their identities should remain unchanged.

methods are often based on graphical network optimization in which the nodes are represented by detection responses. Such methods often fail to handle the problems of long-term tracking in crowded scenes well. To alleviate this, some researchers [19], [25], [26] try to use the track fragments (tracklets) as graph nodes aiming at linking tracklets into long trajectories. This kind of Tracklet Association-based Tracking (TAT) methods can increase robustness and reduce the computation complexity of the graph optimization. There are two key components of a TAT approach: (1) The tracklet affinity model that estimates the likelihood of two tracklets belonging to the same target; (2) The global optimization framework for tracklet association that determines the links of the tracklets based on their affinity scores.

In this paper, we report our algorithm applied to tracking pedestrians in real scenes, but it can be generalized to tracking any other objects in diverse situations. The framework of this approach is shown in Fig. 2.

Given a video sequence, we first detect pedestrians in each frame by an existing detector, such as the Deformable Part Models (DPM) detector [2]. We utilize the strategy introduced in Section 3.1 to generate the initial tracklets, which are mostly reliable. But some errors, though very little, could still exist in initial tracklets. We introduce our target-specific metric learning on these initial tracklets. Then we use the online learned target-specific metrics to refine these initial tracklets for reliable tracklets. The cost-flow network is based on the reliable tracklets and its optimization yields the long-term trajectories of multiple persons. Estimating the transition costs is the key factor in the min-cost network flow optimization. We propose to learn tracklet affinity models, which include weighted discriminative appearance and motion cues, in an online manner for estimating the transition costs.

The main contributions of this paper are: (1) Online learning of target-specific metrics with strong discriminative power through a two-step target-specific metric learning and metric refinement processes. (2) Utilizing both appearance and motion dynamics in the tracklet affinity models, which are updated within each local segment for reduced computation and locally adaptive affinity models. (3) A learning algorithm to learn the weights of motion and appearance tracking cues for tracklet affinity models.

The rest of this paper is organized as follows: Section 2 describes the cost-flow network formulation. Section 3 presents the online learning of the tracklet affinity models. The learning of weights is presented in Section 4. Experimental results and comparisons are shown in Section 5. Section 6 concludes the paper.

2 Cost-Flow Network Formulation for Trajectory Recovery by Tracklet Association

The cost-flow network has been shown to be effective for estimating trajectories in previous studies [11], [12], [13]. However, in these works, the graph nodes are defined by

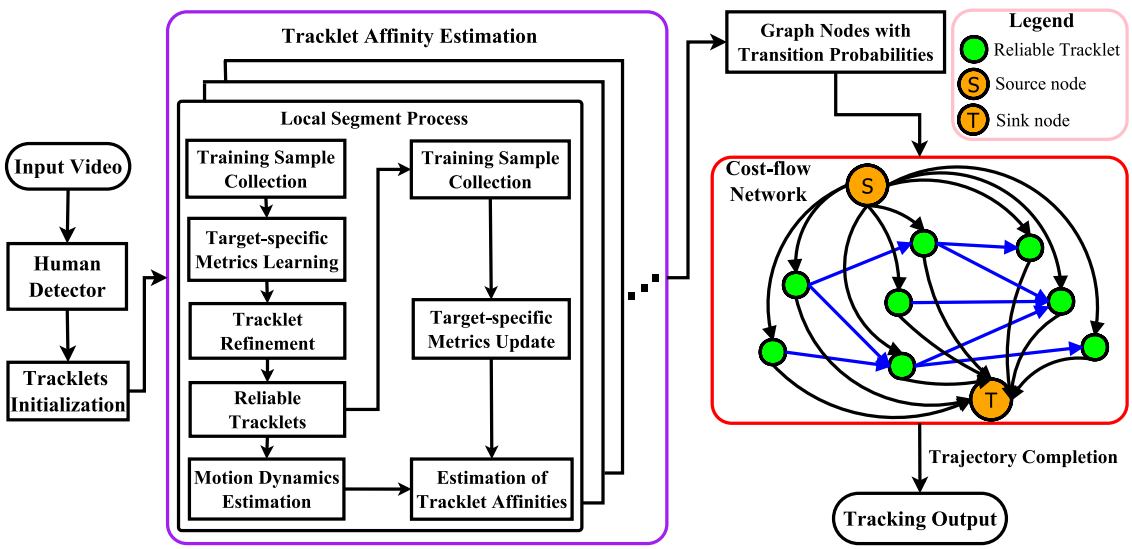

Fig. 2. The proposed framework. In the cost-flow network, each node denotes a reliable tracklet, which is a tracklet with only one identity. The flow costs of edges are defined by negative log of the affinity scores, which are obtained through the online learning of target-specific metrics and motion dynamics with the off-line learned weights on segments of short-time sequences known as local segments.

the detection responses. In recent works [10], [19], [20], [25], [27], [28], Tracklet Association-based Tracking (TAT) methods were proposed for multi-target tracking. In these methods, the tracklets were generated based on association of detection responses. In this paper, we generate the initial tracklets based the successive shortest path algorithm of [13], which will be described in Section 3.1. The initial tracklets are then refined by the proposed online learned target-specific metrics for reliable tracklets. This tracklet refinement process will be presented in Section 3.3. We can construct a smaller graph based on such tracklets which are of a higher order of abstraction than those based on detection responses. The problems in long-term multi-person tracking can be solved by directly linking tracklets instead of detection responses.

An objective function, which takes a similar form as detection association in [11], is defined for tracklet association. Let $X = \{F_i\}$ be the collection of all the tracklets. A single trajectory hypothesis is defined as an ordered list of N tracklets: $T_k = \{F_{k_1}, F_{k_2}, \ldots, F_{k_l}\}$, where $F_{k_i} \in X$, and $i = 1, \ldots, l; 1 \leq l < N$. A tracklet association hypothesis $\mathcal{T}$ is defined as a set of single trajectory hypotheses: $\mathcal{T} = \{T_k\}$.

The objective of tracklet association is to maximize the posteriori probability of $\mathcal{T}$ given X:

$$\begin{aligned} \mathcal{T}^* &= \arg\max_{\mathcal{T}} P(\mathcal{T}|X) \\ &= \arg\max_{\mathcal{T}} P(X|\mathcal{T})P(\mathcal{T}) \\ &= \arg\max_{\mathcal{T}} \prod_i P(F_i|\mathcal{T})P(\mathcal{T}), \end{aligned} \tag{1}$$

assuming that the likelihood probabilities of F_i are conditionally independent.

We take the assumption that the motion of each tracklet is independent and one tracklet can only belong to one trajectory. Then the above equation can be further decomposed into:

$$\mathcal{T}^* = \arg\max_{\mathcal{T}} \prod_i P(F_i|\mathcal{T}) \prod_{T_k \in \mathcal{T}} P(T_k), \tag{2}$$

$$s.t. \quad T_k \bigcap T_l = \phi, \forall k \neq l, \tag{3}$$

where ϕ is the empty set.

The second term in Equ. (2) is defined as follows:

$$\begin{aligned} P(T_k) &= P(\{F_{k_1}, F_{k_2}, \ldots, F_{k_l}\}) \\ &= P_s(F_{k_1}) \left(\prod_{n=1}^{l-1} P(F_{n+1}|F_n) \right) P_t(F_{k_l}), \end{aligned} \tag{4}$$

$P(F_i|\mathcal{T})$ is the likelihood function of tracklet F_i. It is assumed that the false alarm rate is very low from the reliable tracklets, so $P(F_i|\mathcal{T}) \approx 1$. Then Equ. (2) can be further simplified as follows:

$$\begin{aligned} \mathcal{T}^* &= \arg\max_{\mathcal{T}} \prod_i P(F_i|\mathcal{T}) \prod_{T_k \in \mathcal{T}} P(T_k) \\ &= \arg\max_{\mathcal{T}} \prod_{T_k \in \mathcal{T}} P(T_k), \end{aligned} \tag{5}$$

$P(T_k)$ is modeled as a Markov chain, which includes a starting probability $P_s(F_{k_1})$, a termination probability $P_t(F_{k_l})$, and transition probability $P(F_{n+1}|F_n)$ between temporarily adjacent tracklets. Finding the optimal association hypothesis $\mathcal{T}^*$ is equivalent to minimizing the cost of flow from source s to sink t in a network flow graph. A network graph can be constructed as follows:

Given an observation set X: for every tracklet $F_i \in X$, we create a node v_i, an edge from source s to a node,(s, v_i), with cost $c(s, v_i) = c_i^s$ and flow $f(s, v_i) = f_i^s$, and an edge from a node to sink t, (v_i, t) with cost $c(v_i, t) = c_i^t$ and flow $f(v_i, t) = f_i^t$. For every transition $P(F_j|F_i) \neq 0$, create an edge (v_i, v_j) , $i \neq j$, with cost $c(v_i, v_j) = c_{ij}$ and flow $f(v_i, v_j) = f_{ij}$. We take the logarithm of the objective function to simplify the expression while preserving the maximum a posteriori probability (MAP) solution. Then, Equ. (5) can be re-written as follows:

$$\mathrm{T} = \arg\min_{\mathcal{T}} \left(\sum_i c_i^s f_i^s + \sum_{ij} c_{ij} f_{ij} + \sum_i c_i^t f_i^t \right), \tag{6}$$

$$\begin{aligned} &s.t. \quad f_{ij}, f_i^s, f_i^t \in \{0, 1\}, \\ &and \quad f_i^s + \sum_j f_{ji} = f_i^t + \sum_j f_{ij}, \end{aligned} \tag{7}$$

subject to Equ. (6), where

$$\begin{aligned} &c_i^s = -\log P_s(F_i), \quad c_i^t = -\log P_t(F_i), \\ &c_{ij} = -\log P(F_j|F_i). \end{aligned}$$

Equ. (7) ensures that the tracklet association hypothesis $\mathcal{T}$ is non-overlapping. The above formulation can be mapped into a cost-flow network with a source s and a sink t. Estimating the transition costs c_{ij} is very critical in solving this min-cost network flow problem. Previous network flow approaches [11], [12], [13], [16] only utilize motion cues across consecutive frames and simple appearance features such as color histograms to calculate c_{ij}. Nevertheless, these cues are not very reliable when prolonged occlusions and interactions between targets occur. In this paper, we propose to learn the segment-wise tracklet affinity models, consisting of weighted tracking cues, online for estimating c_{ij}.

3 Online Learning of Tracklet Affinity Models

In this section, we introduce the online learning of tracklet affinity models, consisting of online target-specific metric learning and online motion dynamics estimation. The affinity scores of adjacent tracklets, which are used as the transition probabilities between two corresponding nodes in the cost-flow network, can be obtained through tracklet affinity measurements. We perform local transition probabilities estimation within a local segment of S frames ($S = 50$ in our implementation).

In order to obtain effective appearance cues for reliable transition probability estimation, we propose a novel target-specific appearance-based model. The appearance-based model learning problem is formulated as a metric learning problem, which can enhance the features with strong

discriminative power and suppress the features with weak discriminative power. Here, we learn target-specific metrics so that target-specific properties can be efficiently explored for more discriminative models. In contrast to the previous work of [19] in which local descriptors are learned offline, our learning is online throughout and our target-specific metrics are adaptive to local segments. Moreover, to create a more discriminative tracklet affinity model, we also explore the motion dynamics cue and embed it into the proposed tracklet affinity model. The motion dynamics are online estimated without any assumed priors. As a result, the learned tracklet affinity models can better represent the appearance and motion cues adaptively and provide reliable transition probability estimation.

3.1 Initial Tracklet Generation

Before introducing the proposed tracklet affinity models, we first present the initial tracklet generation process. Similar to the cost-flow network formulation described in previous section, the problem of initial tracklet generation is also formulated as a network flow optimization problem. Different from the cost-flow network formulation presented in Section 2, the graph nodes are defined by the detection responses and their costs, referred as local observation costs here, (the negative logarithm of the corresponding detection scores) are added in the formulation. The mathematical formulation of the minimization problem can be expressed as follows:

$$\mathrm{F} = \arg\min\left(\sum_i \hat{c}_i^s \hat{f}_i^s + \sum_{ij} \hat{c}_{ij}\hat{f}_{ij} + \sum_i \hat{c}_i \hat{f}_i + \sum_i \hat{c}_i^t \hat{f}_i^t\right), \quad (8)$$

$$\begin{aligned} &s.t. \quad \hat{f}_{ij}, \hat{f}_i, \hat{f}_i^s, \hat{f}_i^t \in \{0,1\}, \\ &and \quad \hat{f}_i^s + \sum_j \hat{f}_{ji} = \hat{f}_i = \hat{f}_i^t + \sum_j \hat{f}_{ij}, \end{aligned} \quad (9)$$

where $\hat{c}_i^s$, $\hat{c}_i^t$, $\hat{c}_{ij}$, $\hat{c}_i$ denote the starting, termination, transition and local observation costs, respectively. $\hat{f}_i^s$, $\hat{f}_i^t$, $\hat{f}_{ij}$, $\hat{f}_i$ denote the corresponding flows.

To obtain the initial tracklets (relatively short track fragments), the transition cost $\hat{c}_{ij}$ is set to 0 for each candidate detection pair first. Only the detection responses over consecutive frames are considered to be linkable. The transitions of the cost-flow network across non-consecutive frames are not permitted. Moreover, a constraint is imposed on initial tracklet generation. That is, a track fragment should start from a detection response and terminate at a detection response with detection scores higher than a pre-defined threshold, thus only consecutive detection responses with detection scores above the threshold are used to form the initial tracklets. This constraint ensures that the generated initial tracklets are relatively short and mostly reliable track fragments. The dynamic programming algorithm in [13], which approximates the successive shortest path solution, is employed to optimize the cost-flow network. This initial tracklet generation strategy can be viewed as a simplified version of the method in [13]. The average speed of this process is above 500 fps.

3.2 Online Target-Specific Metric Learning

We aim to online learn discriminative target-specific metrics while keeping the computational complexity low. For each tracklet F_i, we learn a distance metric function.

The learning involves feature representation, online training sample collection and online training. To create a strong appearance-based model, we start from a rich set of basic features, which includes color, shape and texture, to describe a pedestrian's appearance.

Given a training dataset $Z = \{z_i^t\}_{i=1}^{N_z}$, where $z_i^t \in \mathbb{R}^{N_d}$ is a feature vector representing the appearance of the image area under the bounding box where there is a strong detection response in tracklet F_i at frame t, N_z is the total number of training samples and N_d is the total number of feature dimensions. The training dataset Z is obtained from reliable tracklets through online training sample collection, which will be introduced in latter part of this section. We define a positive difference vector x_i^p computed between a positive sample pair (a pair of detection responses belonging to the same person) and a negative difference vector x_i^n computed from a negative sample pair (a pair of detection responses belonging to different persons). Here, it is assumed that the first M frames of each initial tracklet are reliable and the detection responses are from the same person. Training samples are therefore collected from these frames. The value of M is empirically determined. It is found that a value M between 6 and 10 frames works well for all sequences. Based on the constraint introduced in previous section, most of the generated initial tracklets are relatively short and mostly reliable. However, some unreliable tracklets may still exist due to occlusions of the targets. This kind of target interactions often occur in the middle of initial tracklets. Based on this observation, we assume that the first M frames of each initial tracklet are mostly reliable.

The difference vectors x_i^p and x_i^n are defined as:

$$\begin{aligned} x_i^p &= d(z_i, z_i') = |z_i - z_i'| \\ x_i^n &= d(z_i, z_j') = |z_i - z_j'|, \quad i \neq j, \end{aligned} \quad (10)$$

where d is an absolute difference function, z_i and z_i' are the feature vectors of two samples from the same tracklet F_i, z_j' is the feature vector of a sample from a different tracklet F_j.

Given the difference vectors x_i^p and x_i^n, a distance function D_i for tracklet F_i can be learned based on relative distance comparison so that $D_i(x_i^p) < D_i(x_i^n)$. This distance function D_i is parameterized as a Mahalanobis distance function:

$$D_i(x) = x^T M_i x, \quad M_i \succeq 0, \quad (11)$$

where M_i is a positive semidefinite matrix.

We adopt the logistic function as in [29] to learn D_i to force $D_i(x_i^p)$ to be small, and $D_i(x_i^n)$ to be big:

$$\min_{D_i} r(D_i) = -\log\left(\left(1 + \exp\left(D_i(x_i^p) - D_i(x_i^n)\right)\right)^{-1}\right). \quad (12)$$

Furthermore, the term M_i in the distance function D_i can be decomposed by eigendecomposition:

$$M_i = A_i \Lambda_i A_i^T = W_i W_i^T, \quad W_i = A_i \Lambda_i^{\frac{1}{2}}, \quad (13)$$

where A_i is the orthonormal eigenvector matrix of M_i and the diagonal of Λ_i are the corresponding eigenvalues.

Therefore, learning a distance function D_i is equivalent to learning the matrix W_i as follows:

$$\begin{aligned} &\min_{W_i} r(W_i), s.t. \quad w_i^T w_j = 0, \forall i \neq j, w_i, w_j \in W_i \\ &r(W_i) = \log\left(1 + \exp\{\|W_i^T x_i^p\|^2 - \|W_i^T x_i^n\|^2\}\right). \end{aligned} \tag{14}$$

Online training sample collection is another important issue in online learning. The q strongest ($q = 4$ in this work) detection responses in each tracklet are used as training samples. For x_i^p, we collect positive sample pairs from the same tracklet. However, for x_i^n, we collect negative sample pairs from different persons. To determine the relevance of sample pairs, two constraints are employed: spatio-temporal and exit constraints. The first constraint is based on the fact that one person cannot appear at two or more different locations at the same time. The second constraint is based on the observation that the person who has already exited the view cannot be the person who is still within the view. We online collect negative samples, which satisfy the above two constraints, from F_i and F_j respectively to form negative sample pairs.

Learning W_i using the optimization criterion (14) is a nonconvex optimization problem. In this work, we utilize the optimization algorithm in [29] to learn W_i for each tracklet F_i. Finally, we obtain the target-specific transform matrices for all the tracklets:

$$W = \{W_i\}, \quad i = 1, \ldots, N. \tag{15}$$

3.3 Tracklet Refinement

To solve the objective function in Equ. (6), we need to identify reliable tracklets for the nodes in the network graph. The strategy of initial tracklet generation, which is described in previous section, uses spatio-temporal information such as distance between corresponding observations in adjacent frames to link the detections into tracklets. Without effective use of appearance cues, the initial tracklets may be not consistent in appearance and hence unreliable when there are many interactions or occlusions between targets. A typical error is that there are some detection responses belonging to different persons in one tracklet. Hence, tracklet refinement is needed to separate tracklets into multiple short but reliable ones.

The online learned target-specific metrics are employed to refine the initial tracklets. To construct the probe set, the detection with the strongest detection response, g_i, is selected from the first M frames of an initial tracklet, F_i, which are assumed to be reliable. It is defined as $G = \{g_i\}$, $i = 1, \ldots, N_s$, where N_s is the number of tracklets in a local segment. Each tracklet F_i has only one selected g_i in G.

We learn the target-specific transform matrix W_i for each initial tracklet after collecting training samples as described in previous section. The identity test is carried out within a local segment frame by frame to obtain the relative distance between the detection response at frame t of F_i and the corresponding g_i in the probe set:

$$\begin{aligned} x_i^t &= d(z_i^t - g_i) = |z_i^t - g_i|; \quad i = 1, \ldots, N_s \\ d_i^t &= \|W_i^T x_i^t\|^2, \end{aligned} \tag{16}$$

where z_i^t is an instance from tracklet F_i at frame t, g_i is the corresponding detection response of F_i in G, and d_i^t is the relative distance between z_i^t and g_i.

To be a reliable tracklet, the relative distance between the current detection response z_i^t and the probe g_i should be small; otherwise, it is an unreliable tracklet. A distance threshold ω is used to identify reliable tracklets. In a tracklet F_i, if K ($K = 5$ in our implementation) consecutive detection responses having relative distance values (from g_i) above ω, we split F_i into two parts from the first consecutive detection response. In virtue of the strategy of initial tracklet generation introduced in Section 3.1, the generated initial tracklets are mostly reliable, but some errors, though very little, could still exist in the initial tracklets. This tracklet refinement process is usually repeated no more than twice to obtain reasonably reliable tracklets.

After obtaining the reliable tracklets, the target-specific metrics learned from the initial tracklets are updated. Different from the training sample collection of initial tracklets that the samples are collected from the first M frames of the tracklets, the training samples of the reliable tracklets are collected from the full-length tracklets. The strategy of online training sample collection is the same as the one introduced in Section 3.2. As shown in Fig. 2, a two-step target-specific metric learning/update is used in the proposed framework. The first step is used for tracklet refinement, which is usually repeated no more than two times. The second step is used for the appearance-based tracklet affinity estimation, which executes only once.

3.4 Online Tracklet Dynamics Estimation

To disambiguate targets with similar appearance, we propose to exploit motion dynamics together with appearance cues as described above to keep track of target's identity. The main idea of tracklet dynamics estimation is to model the evolution of target motions as a sequence of piecewise linear regressors whose orders can be estimated from available data.

The dynamics of a tracklet can be constructed as an ordered sequence of dynamic measurements $\{y_q\}$, $s \leq q \leq e$, where s and e are the starting and ending frames, respectively. Similar to [30], [31], we collect the position information of all the detection responses within one tracklet in a vector y and assume that its value at current time q is related to its past values y_{q-i} by an m^{th} order autoregressive model of the form:

$$\begin{aligned} y_q &= a_1 y_{q-1} + a_2 y_{q-2} + \cdots + a_m y_{q-m} \\ &= \sum_{i=1}^{m} a_i y_{q-i}, \quad m \leq N_f, q \geq s + m, \end{aligned} \tag{17}$$

where $\mathbf{a} = [a_1\ a_2\ , \ldots,\ a_m]^T$ is the regressor vector, N_f is the total number of frames of the tracklet, m is the number of frames of the dynamic measurement y_q and s is the starting frame of the tracklet.

The order of the autoregressive model m measures the complexity of the underlying tracklet dynamics. The goal of tracklet dynamics estimation is, given dynamic measurements $\{y_q\}$, to estimate the minimum m such that the model (17) retains. Specifically, a well known result from the realization theory [32], [33] is that, under mild conditions, given an

ordered sequence of measurements $\{y_q\}$ generated by Equ. (17), the order m of the autoregressive model equals to the rank of the corresponding Hankel matrix, i.e., $m = rank(H_{F_i})$ where H_{F_i} is the Hankel matrix with $n \geq m$ columns:

$$H_{F_i} \doteq \begin{bmatrix} y_s, & y_{s+1} & \cdots & y_{s+n-1} \\ y_{s+1} & y_{s+2} & \cdots & y_{s+n} \\ \vdots & \vdots & \vdots & \vdots \\ y_{t-n+1} & y_{t-n} & \cdots & y_t \end{bmatrix}, \tag{18}$$

where n is defined based on the length of the tracklet:

$$\begin{aligned} n &= l_i - \lceil l_i/3 \rceil + 1; \\ l_i &= t - s + 1, \end{aligned} \tag{19}$$

where l_i is the length of tracklet F_i.

The motion dynamics similarity $P_m(F_i, F_j)$ between two tracklets F_i and F_j, which takes a similar form as in [31], is defined as follows:

$$P_m(F_i, F_j) = \begin{cases} -\infty, & \text{if temporal conflict exists;} \\ \dfrac{rank(H_{F_i}) + rank(H_{F_j})}{rank(H_{F_{ij}})} - 1 & , \end{cases} \tag{20}$$

where $F_{ij} = [F_i \ \alpha_i{}^j \ F_j]$ is the joint tracklet with the gap $\alpha_i{}^j$ between F_i and F_j interpolated. The joint Hankel matrix $H_{F_{ij}}$ is formed by combining the dynamic measurements of F_i, F_j and the interpolated data.

Here, we take the assumption that the targets do not significantly change their dynamics between tracklets. The intuition of the above motion dynamics similarity is that if two tracklets are from the same trajectory then they can be approximated by one relatively low order regressor. Otherwise, if two tracklets are from different trajectories, the joined trajectory needs a higher order regressor than the regressors of each single tracklet. Hence, if $rank(H_{F_i}) = r(F_i)$ and $rank(H_{F_j}) = r(F_j)$, then $rank(H_{F_{ij}}) = r(F_{ij}) \leq (r(F_i) + r(F_j))$. Consequently, if F_i and F_j are of the same trajectory, then $r(F_i) = r(F_j) = r(F_{ij})$ and $P_m(F_i, F_j) = 1$, but if not, $P_m(F_i, F_j) \approx 0$.

Tracklet dynamics are online estimated, without any prior knowledge, based on the reliable tracklets. The IHTLS (Iterative Hankel Total Least Squares) method in [34] is employed to estimate the rank of the Hankel matrices for tracklet dynamics estimation. The computational complexity of rank estimation is $O((l_i - m)m^3)$, where l_i is the length of a tracklet F_i and $m \ll l_i$ is the rank of the matrix.

3.5 Tracklet Affinity Measurement

In this section, we present the measurement of the affinity between F_i and F_j, or equivalently, the transition probability, P_{ij}, in the network graph between node i and node j. The tracklet affinity score, $\mathcal{S}_{ij}$, which is equivalent to P_{ij}, is defined as follows:

$$\mathcal{S}_{ij} = P_m(F_i, F_j) P_a(F_i, F_j) \mathcal{C}_{ij}, \tag{21}$$

where $P_m(F_i, F_j)$ is the motion-based affinity model, which is defined by Equ. (20), $P_a(F_i, F_j)$ is the appearance-based affinity model and $\mathcal{C}_{ij}$ is a limiting function.

To obtain the appearance-based affinity model $P_a(F_i, F_j)$, we first compute the relative distances d_{ij}^t between each detection response in F_i and the probe g_j, and $d_{ji}^{t'}$ between each detection response in F_j and the probe g_i,

$$\begin{aligned} &x_{ij}^t = |z_i^t - g_j|, \ x_{ji}^{t'} = |z_j^{t'} - g_i|; \quad i, j = 1, \ldots, N_s \\ &d_{ij}^t = \|W_i^T x_{ij}^t\|^2, \ d_{ji}^{t'} = \|W_j^T x_{ji}^{t'}\|^2, \end{aligned} \tag{22}$$

where z_i^t denotes the feature vector of a detection response in tracklet F_i at frame t, $z_j^{t'}$ denotes the feature vector of a detection response in tracklet F_j at frame t', and $g_i, g_j \in G$.

Subsequently, we calculate the mean values of the relative distances and use them to define the appearance-based affinity model $P_a(F_i, F_j)$:

$$d_{ij} = \left(\sum_t d_{ij}^t \right) / m, \ d_{ji} = \left(\sum_{t'} d_{ji}^{t'} \right) / n, \tag{23}$$

$$P_a(F_i, F_j) = (d_{ij} d_{ji})^{-1} \gamma, \tag{24}$$

where γ is a normalization term and m, n are the number of frames of F_i and F_j respectively.

We do not have to apply Equ. (21) to every pair, since there are a lot of obviously non-related tracklet pairs which do not belong to the same trajectory. Because a limiting function $\mathcal{C}_{ij}$ is included in Equ. (21), we actually apply it to every tracklet pair. This limiting function $\mathcal{C}_{ij}$ is proposed based on spatio-temporal, and exit constraints:

$$\mathcal{C}_{ij} = C_t(F_i, F_j) C_e(F_i, F_j). \tag{25}$$

The spatio-temporal constraint is defined as follows:

$$C_t(F_i, F_j) = \begin{cases} 1, & \text{if } F_i \cap F_j = \phi \\ 0, & \text{otherwise} \end{cases}, \tag{26}$$

where $\cap$ is an intersection operator that is used to find the overlap between two tracklets and ϕ is the empty set.

The exit constraint is defined based on the observation that the person who has already exited the scene cannot be the person who is still within the scene:

$$C_e(F_i, F_j) = \begin{cases} 1, & \text{if } t_i^s > t_j^e \ \& \ p_j^{t_j^e} \notin E \\ 0, & \text{otherwise} \end{cases}, \tag{27}$$

where t_i^s is the starting frame of tracklet F_i, t_j^e is the ending frame of tracklet F_j, $p_j^{t_j^e}$ is the position of the detection response of tracklet F_j at time t_j^e and E is the exit area which is near image borders. For static cameras, we adopt the incremental learning algorithm for exit map as in [20] to obtain E.

$C_t(F_i, F_j)$ and $C_e(F_i, F_j)$ associate F_i and F_j if they have no overlap and F_i does not exit the screen when F_j appears.

The transition costs of the adjacent nodes in the cost-flow network is obtained by taking negative logarithm of the affinity scores between corresponding tracklets:

$$c_{ij} = -\log \mathcal{S}_{ij}. \tag{28}$$

Finally, we can estimate the optimal tracklet association hypothesis $\mathcal{T}^*$ in Equ. (6) based on c_{ij}. Although the transition costs c_{ij} are estimated within local segments, the final tracking trajectories are obtained through network flow optimization on the whole sequence. After tracklet association, there may exist some gaps between adjacent tracklets in each trajectory due to missed detections and occlusions. The possible gaps in the tracking trajectories are interpolated linearly.

However, in the proposed tracklet affinity model as depicted in Equ. (21), the motion-based affinity model, $P_m(F_i, F_j)$, and appearance-based affinity model, $P_a(F_i, F_j)$, are treated equally without any voting weights. This may result in inaccurate affinity scores if one of the tracking cues is dominant and the other one is confusing, having an effect as a noise factor. Therefore, we investigate the influences of the two tracking cues on tracking performance in next section.

4 Learning of Affinity Weights

In difficult situations, where severe occlusions and interactions occur, the motion-based affinity model and appearance-based affinity model may not be consistent. Hence, we need to weight them properly for stable performance.

We propose to add a weighting parameter λ, which controls the weight of the motion-based affinity score, in Equ. (21).

$$\mathcal{S}_{ij} = [P_m(F_i, F_j)]^{\lambda} P_a(F_i, F_j) \mathcal{C}_{ij}, \quad 0 \leq \lambda \leq 1, \tag{29}$$

where λ is learned from labeled data. If the value of λ is larger, the motion-based affinity score, $P_m(F_i, F_j)$, contributes more to $\mathcal{S}_{ij}$.

4.1 Assessment of Difficult Situations for Motion Dynamics

To investigate the difficult situations where the motion affinities are not reliable, we only utilize the motion-based affinity model to estimate c_{ij} for Equ. (6) in the experiments. After analyzing the inconsistencies between the tracking results and the labeled ground truth data, we obtain these typical situations where the motion affinities are not reliable. Based on the analysis, we design a rule to automatically assess these difficult situations.

There are two constraints in this rule. The first one is that two tracklets should have a certain amount of overlap in the starting or ending frames, which indicates the occlusion of two targets:

$$\begin{aligned} &S(z_i^{t^e}) \cap S(z_k^{t^e}) \geq \eta * \min(S(z_i^{t^e}), S(z_k^{t^e})) \text{ or} \\ &S(z_i^{t^s}) \cap S(z_k^{t^s}) \geq \eta * \min(S(z_i^{t^s}), S(z_k^{t^s})), \end{aligned} \tag{30}$$

where $z_i^{t^e}$ and $z_i^{t^s}$ are the detection responses of F_i at the ending frame t^e and the starting frame t^s, respectively. $z_k^{t^e}$ and $z_k^{t^s}$ are the detection responses of F_k at the ending frame t^e and the starting frame t^s, respectively. $S(\cdot)$ is the operator to capture the area of the detections in pixels. η is a sensitivity threshold ($\eta = 0.3$ in our implementation).

The second constraint is that tracklets F_i and F_j must have a gap for it to be linkable. That is,

Fig. 3. An example of the difficult situations.

$$t_j^s - t_i^e > 1, \quad i \neq j, \tag{31}$$

where t_j^s is the starting frame of tracklet F_j, t_i^e is the ending frame of tracklet F_i, and $t_j^s > t_i^e$.

If the tracklet pair $\{F_i, F_k\}$ match the above two conditions, then we add the weighting parameter λ to the motion-based affinity models related to F_i and F_k as $[P_m(F_i, F_j)]^{\lambda}$ and $[P_m(F_k, F_l)]^{\lambda}$. F_j, F_l are the linked candidate tracklets of F_i and F_k respectively. As we can see in Fig. 3, the tracklet pairs with identities 269, 289 and 305, 306 match these two constraints. In such situation, due to interactions of the two targets, the two corresponding trajectories become ambiguous. Hence, we add the weighting parameter λ for these four tracklets in terms of the motion-based affinity models.

4.2 Learning of the Weighting Parameter

The weighting parameter λ in Equ. (29) defines the weight of the motion-based affinity model for tracklet association. Based on the number of frames of the gaps between tracklets, we divide λ into 2 levels:

$$\lambda = \begin{cases} \lambda_1, & 1 \leq u \leq B_1 \\ \lambda_2, & u > B_1 \end{cases}, \tag{32}$$

where u is the number of frames in the gap between corresponding tracklets ($B_1 = 20$ in our implementation).

The intuition is that if the gaps are longer, it is more difficult to accurately estimate the joint tracklet dynamics. Therefore, we define 2 difficulty levels as in Equ. (32), making the weighting parameter λ adaptive

to the difficult situations. The number of difficulty levels and the upper bound value of level 1 (B_1) are empirically determined. Furthermore, we employ tracking performance evaluation and network flow optimization jointly to optimize the weighting parameters for tracklet association.

Algorithm 1. Weighting Parameter Learning for Tracklet Association

Input:
Reliable tracklets;
Labeled ground truth data;
Output:
The learned weighting parameters: $\{\lambda_1, \lambda_2\}$;
Initialize the weighting parameters:
$\lambda_1 = \lambda^l{}_1 = 0, \lambda_2 = \lambda^l{}_2 = 0$ and the step value $\Delta\lambda = 0.1$;
Online estimate transition costs for all graph node (tracklet) pairs based on:
$c_{ij} = -\log(P_m(F_i, F_j)P_a(F_i, F_j)\mathcal{C}_{ij})$;
for i=1 to 2 **do**
  while $\lambda^l{}_i \leq 1$ **do**
    for all graph node (tracklet) pair $\{F_i, F_k\}$ matches the rule of the assessment of difficult situations **do**
      if $u \geq 1$ and $u \leq B_1$ **then**
        $\lambda = \lambda_1$;
      else if $u > B_1$ **then**
        $\lambda = \lambda_2$;
      end if
      for all tracklet pairs related to F_i, F_k **do**
        $c_{ij} = -\log([P_m(F_i, F_j)]^{\lambda} P_a(F_i, F_j)\mathcal{C}_{ij})$;
        $c_{kl} = -\log([P_m(F_k, Fl)]^{\lambda} P_a(F_k, F_l)\mathcal{C}_{kl})$;
      end for
    end for
    Obtain tracking results through network flow optimization;
    if Current tracking results better converge to ground truth data **then**
      $\lambda_i = \lambda^l{}_i$;
    end if
    $\lambda^l{}_i = \lambda^l{}_i + \Delta\lambda$;
  end while
end for
return $\{\lambda_1, \lambda_2\}$.

The learning algorithm is summarized in Algorithm 1. Given the reliable tracklets and the labeled ground truth data of a video sequence, we aim to learn the weighting parameters in a supervised manner so that the tracking performance can be optimized. The two proposed weighting parameters are optimized independently in a greedy fashion. The weighting parameters are initialized as $\lambda_1 = 0, \lambda_2 = 0$. After some iterations with a fixed step value, the weighting parameters $\{\lambda_1, \lambda_2\}$ are obtained.

The weighting parameters λ_1 and λ_2 are learned from the ground truth data of PETS 2009 [35] in this paper. Our tracking algorithm is then run with the learned weighting parameters ($\lambda_1 = 0.5, \lambda_2 = 0.2$) on all the datasets for evaluation. Based on the analysis of the experimental results with different B_1, we find that the tracking performance is slightly affected by the changes of B_1. An upper bound value B1 of (20-30) frame gap works well for all sequences.

5 Experiments

5.1 Datasets

To evaluate the performance of the proposed approach, we experiment on five challenging, publicly available pedestrian datasets.

TUD. The TUD Crossing sequence [36] and TUD-Stadtmitte sequence [37] are real-world videos filmed in busy pedestrian streets. The cameras are positioned at a quite low angle, resulting in more complex occlusion patterns and rather inaccurate ground plane locations. Furthermore, for TUD-Stadtmitte, the size of the pedestrians on the image plane vary drastically.

PETS 2009. This benchmark dataset [35] presents an outdoor scene with large number of pedestrians captured from multiple cameras at 7 fps. The pedestrians vary significantly in appearance due to shadows and lighting changes. Moreover, there are frequent occlusions, caused by pedestrian occluding each other, or static occlusions such as the traffic sign. In the experiments, we use the sequences S2L1 and S2L2 in the first view, which are widely used in literature.

Town Centre. The Town Centre dataset [38] is captured by a single elevated camera in a busy street. There are 16 pedestrians visible at any time on average, leading to frequent dynamic occlusions and interactions. Furthermore, due to the severe occlusions caused by static obstacles, many pedestrians are not detected by the state-of-the-art detectors.

ETH. The ETH BAHNHOF and SUNNY DAY sequences [39] show busy street scenes from a pair of cameras on a moving stroller. The stroller is moving forward at most of the time, however there are still some panning motions, which leads to the unreliable motion affinities between tracklets. Moreover, frequent full or partial occlusions occur due to the low view angles of cameras. The size of the pedestrians also varies significantly on the image plane.

MOTChallenge. The MOTChallenge 2D Benchmark is an up-to-date multiple object tracking benchmark. It consists of a total of 22 sequences, in which half of them are used for training and half of them are used for testing. The test sequences cover many different situations, such as different viewpoints, static or moving camera, different weather conditions. This makes MOTChallenge benchmark very challenging.

5.2 Experimental Settings

The online collected training samples from video frames are normalized to 128×64 pixels for target-specific metric learning. For the color feature, RGB, YCbCr and HSV color histograms are extracted with 16 bins for each channel respectively and concatenated into a 144-element vector. To capture shape information, we adopt the Histogram of Gradients (HOG) feature [1] by setting the cell size to be 8 to form a 3968-element vector. Two types of texture features are extracted by Schmid and Gabor filters. In total, 13 Schmid channel features and eight Gabor channel features are obtained to form a 336-element vector by using a 16-bin histogram vector to represent each channel. Each person image is thus represented by a feature vector in a 4448-dimensional feature space.

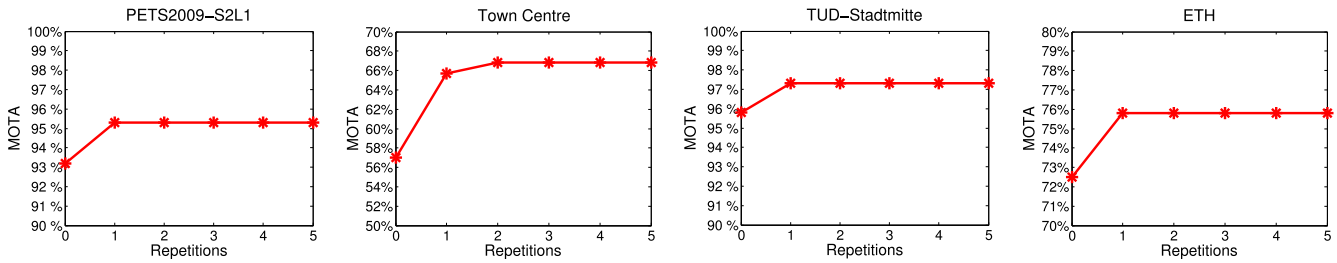

Fig. 4. Influence of tracklet refinement process on tracking performance. Each plot presents the performance (measured by MOTA score) on a particular dataset w.r.t. the number of repetitions of tracklet refinement process.

5.3 Evaluation Metrics

Since it is difficult to use one single score to evaluate multi-target tracking performance, we utilize the evaluation metrics defined in [9], [16], as well as the standard CLEAR MOT metrics [40]:

- *MOTA*(↑): Multi-object tracking accuracy.
- *MOTP*(↑): Multi-object tracking precision.
- *Recall*(↑): correctly matched detections / total detections in ground truth.
- *Precision*(↑): correctly matched detections / total detections in the tracking result.
- *FAF*(↓): number of false alarms per frame.
- *GT*: number of trajectories in ground truth.
- *MT*(↑): number of mostly tracked trajectories.
- *PT*: number of partially tracked trajectories.
- *ML*(↓): number of mostly lost trajectories.
- *Frag*(↓): number of fragmentations.
- *IDS*(↓): number of id switches.
- *IDS/correctly matched detections* (↓).

For evaluation measures with (↑), higher scores denote better performance; for evaluation measures with (↓), lower scores denote better performance. A tracking bounding box in the result having more than 50 percent overlap with the corresponding groundtruth bounding box is considered as true positive. The evaluation codes are downloaded from [41].

5.4 Influence of Tracklet Refinement

To investigate the influence of the repetitions of tracklet refinement process, we run our tracking algorithm and experimented with different number of repetitions while keeping all the other conditions fixed. As shown in Fig. 4, for each dataset, the changes in performance (measured by MOTA score) is plotted against the repetitions of tracklet refinement process. 0 repetitions in Fig. 4 means that no tracklet refinement is utilized for our tracking algorithm. Note that the tracking performance has been improved by exploiting the tracklet refinement for all datasets. Moreover, it is found that the optimal tracking performance is achieved by no more than two repetitions of tracklet refinement process for the four exemplar datasets. From the statistics as shown in Fig. 4, we can conclude that the proposed tracking algorithm with only one time tracklet refinement process can achieve near-optimal tracking performance.

5.5 Quantitative Evaluation

The quantitative evaluations are presented in three sections: abbreviations of the proposed methods in the experiments, comparison with network flow based methods, and comparison with other state-of-the-art methods on benchmark datasets. The tracking results of other methods are extracted from the published papers and the MOTChallenge benchmark website [42] for the ease of reference.

5.5.1 Abbreviations of Different Methods

- *CML:* The proposed method with only an online learned common class metric for all tracklets.
- *TSML:* The proposed method with online target-specific metric learning.
- *TD:* The proposed method with only tracklet dynamics.
- *TSML+TD:* The proposed method with online target-specific metric learning and tracklet dynamics.
- *TSML+TD+WP:* The proposed method with full tracklet affinity model including target-specific metric learning (*TSML*), tracklet dynamics (*TD*) and weighting parameters (*WP*).

CML and *TSML* are from our previous work [18].

5.5.2 Comparison with Network Flow Based Methods

We first evaluate our method on the popular TUD Crossing sequence [36] and ETH BAHNHOF sequence [39]. For a fair comparison, we use the same sequences and pre-trained pedestrian detector as used in [16]. The quantitative metric that we use is *ID switches / total number of correct observations used in the trajectories (IDS / correctly matched detections)*, which is the same as in [16]. Table 1 gives the quantitative results computed on the TUD Crossing sequence, and the first 350 frames of the ETH BAHNHOF sequence. Due to the forward and panning motions of the cameras, the

TABLE 1
Comparison of Tracking Results with Network Flow Based Methods on TUD Crossing and ETH BAHNHOF (First 350 Frames) Sequences

Algorithm	TUD Crossing	ETH	ETH (GT)
DP [13]	32/768	37/1387	25/1648
MCNF [11]	9/433	11/1057	5/922
LRMCNF [16]	14/819	23/1514	14/1783
CML	10/845	5/1728	3/1786
TSML	7/862	1/1790	0/1820

The entries in the table are (IDS)/(correctly matched detections). Columns 1 and 2 use the pre-trained human detector of [3]. Column 3 shows the results when ground truth bounding boxes are used to generate the initial tracklets. The ground truth bounding boxes are from [43].

TABLE 2
Comparison of Tracking Results between State-of-the-Art Methods and Ours on PETS2009-S2L1

Method	MOTA	MOTP	Recall	Precision	FAF	GT	MT	PT	ML	Frag	IDS
Energy Minimization [45]	81.4%	76.1%	-	-	-	19	82.6%	17.4%	**0.0%**	21	15
DC Tracking [15]	95.9%	78.7%	-	-	-	19	**100.0%**	0.0%	**0.0%**	8	10
KSP [12]	80.3%	72.0%	-	-	-	19	73.9%	17.4%	8.7%	22	13
MTMM [46]	83.3%	71.1%	-	-	-	19	89.5%	10.5%	**0.0%**	45	19
UHMTGDA [47]	97.8%	75.3%	-	-	-	19	**100.0%**	0.0%	**0.0%**	8	8
HJMRMT [48]	98.0%	82.8%	-	-	-	19	**100.0%**	0.0%	**0.0%**	11	10
$(MP)^2T$ [49]	90.7%	76.0%	-	-	-	19	-	-	-	-	-
DTLE Tracking [50]	90.3%	74.3%	-	-	-	19	78.3%	21.7%	**0.0%**	15	22
CEMMT [51]	90.6%	80.2%	-	-	-	19	91.3%	4.4%	4.3%	**6**	11
GMCP-Tracker [52]	90.3%	69.0%	-	-	-	19	89.5%	10.5%	**0.0%**	54	10
OMTD [14]	79.7%	56.3%	-	-	-	-	-	-	-	-	-
OMAT [53]	92.8%	74.3%	-	-	-	19	**100.0%**	0.0%	**0.0%**	11	8
PMPTCS [54]	76.0%	53.8%	-	-	-	-	-	-	-	-	-
OGOMT [55]	**98.1%**	80.5%	-	-	-	19	**100.0%**	0.0%	**0.0%**	16	9
CSL-VOX [56]	89.78%	-	**98.28%**	91.07%	-	19	-	-	-	-	6
CSL-DPT [56]	88.13%	-	97.64%	90.45%	-	19	-	-	-	-	8
CML	92.1%	**86.4%**	95.1%	97.6%	0.14	19	94.7%	5.3%	**0.0%**	26	28
TSML	93.4%	**86.4%**	96.0%	97.7%	0.13	19	94.7%	5.3%	**0.0%**	21	18
TD	93.7%	86.3%	96.6%	97.4%	0.15	19	94.7%	5.3%	**0.0%**	17	13
TSML+TD	94.7%	**86.4%**	97.2%	97.6%	0.14	19	94.7%	5.3%	**0.0%**	12	7
TSML+TD+WP	95.3%	**86.4%**	97.4%	**98.0%**	**0.11**	19	94.7%	5.3%	**0.0%**	11	**4**

motion affinities between tracklets are unreliable for the BAHNHOF sequence. Therefore, we do not add the online tracklet dynamics estimation for the experiments in this section. We report the results of five methods: DP algorithm of [13] is our baseline work without adding the online learning of tracklet affinity models. The results are also compared to those of other network flow based methods: MCNF [11] and LRMCNF [16]. The proposed method with online target-specific metric learning is denoted as TSML. Furthermore, we also report the results of the proposed method with only a common class metric for all tracklets, which is denoted as CML.

Note that our method gives better results when compared with the three network flow methods [11], [13], [16]. Moreover, the noticeable improvement in ID switches indicates that our method can better deal with long-term tracking, where the traditional motion models are less reliable.

5.5.3 Comparison with State-of-the-Art Methods

To show the effectiveness of our method, we further compare our method with other state-of-the-art methods on more publicly available datasets. We use the pre-trained human detector of [3] to generate the detections. For the MOTChallenge benchmark [44], we utilize DPM detections [3] and the public detections from this benchmark for the evaluation. In the result tables, the numbers ranked in the first place of the respective evaluation measures are marked in bold.

PETS2009-S2L1. For a fair comparison, we utilize the same ground truth as in [51] for the experiments, in which all the occurring pedestrians have been annotated. The quantitative results are shown in Table 2. As expected, taking tracklet dynamics into account increases the overall tracking performance. Our full tracklet affinity model (TSML+TD+WP) further raises the MOTA by 0.6 percent and reduces the ID switches by ≈ 43 percent. This indicates that our method with full tracklet affinity model combines motion and appearance cues properly, resulting in further improvement on tracking performance. On the whole, our method with full tracklet affinity model achieves the best performance compared with 16 state-of-the-art methods in terms of MOTP, Precision, FAF, ML and IDS. For other evaluation measures, our approach also achieves comparative performance.

Town Centre. To show the generality of the learned weighting parameters, we evaluate our approach with the learned weighting parameters on Town Centre dataset. The ground truth we used here is provided by [38], which is the same as in the compared methods. Due to severe occlusions caused by static obstacles (such as benches) and more frequent dynamic interactions between pedestrians, many pedestrians cannot be detected by the state-of-the-art detectors. Hence, the Recall (as shown in Table 3) is lower than the other datasets. As we can see in Table 3, the full tracklet affinity model with the weighting parameters achieves better or nearly the same performances on all evaluation items. Compared with the tracklet affinity model without weighting parameters, the MOTA is improved by about 8.4 percent; recall and precision are improved by about 1.6 and 3.4 percent respectively; fragments and ID switches are reduced by 23.6 and 24.3 percent respectively. The obvious improvements in performance indicate that the learned weighting parameters are applicable to new data.

TUD-Stadtmitte. To make a fair comparison, the experiments are conducted using the same ground truth as defined in [25]. The quantitative tracking results are shown in Table 4. Though there are occlusions and interactions between pedestrians, the number of pedestrians appearing in the scene is less than other datasets. Hence, our method can generate better optimal tracking results on TUD-Stadtmitte than other datasets. Note that our proposed method with target-specific metric learning (TSML) has achieved very good performance. We also provide the tracking results of the proposed method with TSML+TD and TSML

TABLE 3
Comparison of Tracking Results between State-of-the-Art Methods and Ours on Town Centre Dataset

Method	MOTA	MOTP	Recall	Precision	FAF	GT	MT	PT	ML	Frag	IDS
$(MP)^2T$ [49]	**75.7%**	71.6%	-	-	-	231	-	-	-	-	-
SGB Tracker [57]	71.3%	71.8%	-	-	-	231	58.6%	34.4%	7.0%	363	165
GMCP-Tracker [52]	75.6%	71.9%	-	-	-	231	-	-	-	-	-
MCNF [11]	69.1%	72.0%	-	-	-	231	53.0%	37.7	9.3%	440	243
SMT [38]	64.3%	**80.2%**	-	-	-	231	**67.4%**	26.1%	**6.5%**	343	222
MSBMT [58]	65.5%	71.8%	-	-	-	231	59.1%	33.9%	7.0%	499	288
OMAT [53]	69.5%	68.7%	-	-	-	231	64.7%	27.4%	7.9%	453	209
WAYWAG [59]	66.6%	71.7%	-	-	-	231	58.1%	35.4%	**6.5%**	492	302
OGOMT [55]	70.7%	68.6%	-	-	-	231	56.3%	36.3%	7.4%	321	**157**
CML	55.3%	72.6%	69.9%	86.5%	1.79	231	52.8%	36.4%	10.8%	508	327
TSML	57.3%	72.9%	72.3%	87.5%	1.58	231	60.2%	30.7%	9.1%	326	269
TD	55.7%	73.2%	71.5%	86.9%	1.71	231	55.8%	34.2%	10.0%	362	264
TSML+TD	61.6%	74.3%	74.0%	89.5%	1.38	231	61.9%	29.9%	8.2%	259	214
TSML+TD+WP	66.8%	74.4%	**75.2%**	**92.5%**	**0.96**	231	64.9%	28.2%	6.9%	**198**	162

TABLE 4
Comparison of Tracking Results between State-of-the-Art Methods and Ours on TUD Stadtmitte Dataset

Method	MOTA	MOTP	Recall	Precision	FAF	GT	MT	PT	ML	Frag	IDS
Energy Minimization [45]	-	-	-	-	-	9	60.0%	30.0%	**0.0%**	4	7
DC Tracking [15]	-	-	74.7%	84.2%	0.870	10	50.0%	50.0%	**0.0%**	8	10
PRIMPT [19]	-	-	81.0%	**99.5%**	**0.028**	10	60.0%	30.0%	10.0%	**0**	1
Online CRF Tracking [25]	-	-	87.0%	96.7%	0.184	10	70.0%	30.0%	**0.0%**	1	**0**
CML	94.5%	**72.7%**	95.1%	99.4%	0.030	10	**100%**	0.0%	**0.0%**	2	1
TSML	**97.3%**	71.3%	**98.0%**	99.3%	0.040	10	**100%**	0.0%	**0.0%**	3	**0**
TSML+TD	**97.3%**	71.3%	**98.0%**	99.3%	0.040	10	**100%**	0.0%	**0.0%**	3	**0**
TSML+TD+WP	**97.3%**	71.3%	**98.0%**	99.3%	0.040	10	**100%**	0.0%	**0.0%**	3	**0**

TABLE 5
Comparison of Tracking Results between State-of-the-Art Methods and Ours on ETH Dataset

Method	MOTA	MOTP	Recall	Precision	FAF	GT	MT	PT	ML	Frag	IDS
PRIMPT [19]	-	-	76.8%	86.6%	0.891	125	58.4%	33.6%	8.0%	23	11
Online CRF Tracking [25]	-	-	79.0%	90.4%	0.637	125	68.0%	24.8%	7.2%	**19**	11
DTLE Tracking [50]	-	-	77.3%	87.2%	-	125	66.4%	25.4%	8.2%	69	57
LIMC Tracking [60]	-	-	**83.8%**	79.7%	-	125	**72.0%**	23.3%	**4.7%**	85	71
CML	71.6%	77.0%	78.7%	92.0%	0.710	125	60.0%	29.6%	10.4%	77	19
TSML	**75.8%**	**77.2%**	80.9%	**94.2%**	**0.520**	125	65.6%	24.0%	10.4%	26	**5**

Note that the forward and panning motions of the cameras lead to unreliable motion affinities between tracklets of this dataset. We thus do not employ TD and WP in the experiment.

+TD+WP, which show the same optimal tracking results as shown in Table 4. Compared with [19], [25], the improvement is obvious for some metrics. Our method achieves the highest recall and the mostly tracked score (MT) among all the methods. It also achieves the lowest ID switches. Meanwhile, our method achieves competitive performance on precision, false alarms per frame and fragments compared with [19], [25].

ETH. To see the effectiveness of the proposed method, we further evaluate it on the challenging ETH dataset [39]. Due to the unreliable motion affinities between tracklets of this dataset, we use the tracklet affinity model without TD and WP for the experiments. For a fair comparison, we use the ground truth provided by [25]. The quantitative tracking results are shown in Table 5. We can see that our method can achieve better or competitive performance on all the commonly used evaluation measures. Compared with [19], the most related work, the recall and precision are improved by 4.1 and 7.6 percent respectively; the MT is improved by 7.2 percent; false alarms per frame are reduced by 41.6 percent; and ID switches are reduced by 54.5 percent. The significant reduction in ID switches and false alarms indicates that our target-specific appearance-based model is superior to the method by [19].

MOTChallenge 2D Benchmark. To further show more meaningful quantitative evaluation of the proposed method, we evaluate it on the recent MOTChallenge 2D Benchmark [44]. The number of test sequences in this benchmark is 11, in which 5 of them are taken by moving cameras and 6 of them are taken by static cameras. For the sequences taken by static cameras, our full tracklet affinity model (TSML+TD+WP) is used for evaluation. Due to the moving cameras, the motion affinities estimated by proposed tracklet dynamic model are not reliable. Hence, for

TABLE 6
Comparison of Tracking Results between State-of-the-Art Methods and Ours on MOTChallenge 2D Benchmark

Method	MOTA	MOTP	FAF	GT	MT	PT	ML	Frag	IDS
DP_NMS [13]	14.5%	70.8%	2.3	721	6.0%	53.2%	40.8%	3090	4537
TC_ODAL [61]	15.1%	70.5%	2.2	721	3.2%	41%	55.8%	1716	637
CEM [51]	19.3%	70.7%	2.5	721	8.5%	45%	46.5%	1023	813
SMOT [34]	18.2%	71.2%	1.5	721	2.8%	42.4%	54.8%	2132	1148
TBD [62]	15.9%	70.9%	2.6	721	6.4%	45.7%	47.9%	1963	1939
LP2D [44]	19.8%	71.2%	2.0	721	6.7%	52.1%	41.2%	1712	1649
RMOT [63]	18.6%	69.6%	2.2	721	5.3%	41.4%	53.3%	1282	684
Ours1	**49.1%**	**74.3%**	**0.9**	721	**30.4%**	43.2%	**26.4%**	1034	637
Ours2	34.3%	71.7%	1.4	721	14.0%	46.6%	39.4%	**959**	**618**

"Our1" uses the DPM detections [3]. "Ours2" uses the public detections from this benchmark [42].

TABLE 7
Comparison of Tracking Results between State-of-the-Art Methods and Ours on PETS2009-S2L2

Method	MOTA	MOTP	FAF	GT	MT	PT	ML	Frag	IDS
DP_NMS [13]	33.8%	69.4%	2.2	42	7.1%	83.4%	9.5%	705	1029
TC_ODAL [61]	30.2%	69.2%	2.5	42	2.4%	78.6%	19.0%	499	284
CEM [51]	44.9%	70.2%	1.5	42	11.9%	73.8%	14.3%	**165**	**150**
SMOT [34]	34.4%	70.0%	**1.1**	42	0.0%	76.2%	23.8%	514	251
TBD [62]	35.5%	69.2%	3.1	42	7.1%	78.6%	14.3%	480	523
LP2D [44]	40.7%	70.2%	1.9	42	9.5%	73.8%	16.7%	359	319
RMOT [63]	37.2%	67.7%	2.6	42	9.5%	76.2%	14.3%	320	190
Ours1	**59.7%**	**74.4%**	2.3	42	**31.0%**	64.2%	**4.8%**	200	173
Ours2	51.5%	70.6%	2.1	42	14.3%	76.2%	9.5%	198	165

"Our1" uses the DPM detections [3]. "Ours2" uses the public detections from [42].

the sequences taken by moving cameras, our proposed method with only target-specific metric learning (TSML) is used for evaluation. To further show the generalization capability of the learned weighting parameters, the same parameters $\lambda_1 = 0.5, \lambda_2 = 0.2$ are used for all the 6 testing sequences taken by static cameras. The evaluation results are generated from the MOTChallenge benchmark website [42]. Hence, only the optimal results of the proposed method are provided. As shown in Table 6, compared with other state-of-the-art methods, our method achieves better or competitive performance on all the evaluation measures.

PETS2009-S2L2. To show the effective of the proposed method on more crowded sequences in PETS 2009 dataset, we further evaluate our method on PETS2009-S2L2 sequence. The evaluation result is generated from the MOTChallenge benchmark website [42]. As shown in Table 7, our method achieves the best performance on MOTA, MOTP, MT and ML compared with other state-of-the-art methods. For other evaluation items, our method also achieves competitive performance.

5.6 Computational Speed

The computation speed depends on the number of targets in a video sequence. Our method is implemented using MATLAB on a 3.3 GHz, 4 core PC with 8 GB memory. The speed of the proposed method with target-specific metric learning (TSML) is about 13, 6, 10 and 9 fps for PETS 2009, Town Centre, TUD and ETH datasets, respectively, excluding the detection time; for PETS 2009 and Town Centre datasets, the speed of the proposed method with our full tracklet affinity model is 11 and 5 fps respectively. The average speed of the proposed method on MOTChallenge 2D Benchmark is about 7 fps. The online learning of tracklet affinity models is the most time consuming part of our method, which takes up about 90 percent of the total computation time. The breakdown is as follows: the learning of appearance-based tracklet affinity model and motion dynamics estimation take up about 80 and 10 percent respectively. Speed-up can be achieved by parallel implementations of the online learning of target-specific metrics. Furthermore, the learning of appearance-based tracklet affinity model and motion dynamics estimation can also be implemented in parallel.

6 Conclusion

We have presented our method developed for tracking multiple objects of interest in the scene over a longer period with the aim to maintain consistent tracking and tagging of objects, reducing identity switches. Our method processes the initial tracklets (track fragments) produced by a simple trajectory based tracking algorithm. We propose a two-step online target-specific metric learning to improve the similarity measure based on the appearance cues, and together with coherent dynamics estimation for tracklets based on the motion cues, we establish our new affinity model. The tracking of objects is accomplished by performing tracklet association with network flow optimization where the nodes in the network are tracklets. Thus, our proposed method exploiting both appearance and motion cues is capable to prevent identity switches during tracking and recover missed detections. Our method is found to be effective even when the appearance or motion cues fail to identify or follow the target due to occlusions or object-to-object interactions. To further improve our method, we also

propose to learn the weights of these two tracking cues in our affinity model. Our tracking algorithm has been validated on several public datasets and the experimental results show that it outperforms several state-of-the-art tracking algorithms.

ACKNOWLEDGMENTS

The authors would like to acknowledge the Research Scholarship from School of EEE, Nanyang Technological University, Singapore.

REFERENCES

[1] N. Dalal and B. Triggs, "Histograms of oriented gradients for human detection," in *Proc. IEEE Comput. Soc. Conf. Comput. Vision Pattern Recognition*, 2005, pp. 886–893.
[2] P. Felzenszwalb, D. McAllester, and D. Ramanan, "A discriminatively trained, multiscale, deformable part model," in *Proc. IEEE Conf. Comput. Vision Pattern Recognition*, 2008, pp. 1–8.
[3] P. Felzenszwalb, R. Girshick, D. McAllester, and D. Ramanan, "Object detection with discriminatively trained part based models," *IEEE Trans. Pattern Anal. Mach. Intell.*, vol. 32, no. 9, pp. 1627–1645, Sep. 2010.
[4] C. Huang and R. Nevatia, "High performance object detection by collaborative learning of joint ranking of granule features," in *Proc. IEEE Conf. Comput. Vision Pattern Recog.*, 2010, pp. 41–48.
[5] O. Tuzel, F. Porikli, and P. Meer, "Human detection via classification on Riemannian manifolds," in *Proc. IEEE Conf. Comput. Vision Pattern Recog.*, 2007, pp. 1–8.
[6] X. Wang, T. X. Han, and S. Yan, "An HOG-LBP human detector with partial occlusion handling," in *Proc. IEEE Conf. Comput. Vision Pattern Recog.*, 2009, pp. 32–39.
[7] B. Wu and R. Nevatia, "Detection of multiple, partially occluded humans in a single image by Bayesian combination of edgelet part detectors," in *Proc. IEEE Conf. Comput. Vision Pattern Recog.*, 2005, pp. 90–97.
[8] C. Huang, B. Wu, and R. Nevatia, "Robust object tracking by hierarchical association of detection responses," in *Proc. Eur. Conf. Comput. Vision*, 2008, pp. 788–801.
[9] Y. Li, C. Huang, and R. Nevatia, "Learning to associate: Hybridboosted multi-target tracker for crowded scene," in *Proc. IEEE Conf. Comput. Vision Pattern Recog.*, 2009, pp. 2953–2960.
[10] J. Xing, H. Ai, and S. Lao, "Multi-object tracking through occlusions by local tracklets filtering and global tracklets association with detection responses," in *Proc. IEEE Conf. Comput. Vision Pattern Recog.*, 2009, pp. 1200–1207.
[11] L. Zhang, Y. Li, and R. Nevatia, "Global data association for multi-object tracking using network flows," in *Proc. IEEE Conf. Comput. Vision Pattern Recog.*, 2008, pp. 1–8.
[12] J. Berclaz, F. Fleuret, E. Turetken, and P. Fua, "Multiple object tracking using K-shortest paths optimization," *IEEE Trans. Pattern Anal. Mach. Intell.*, vol. 33, no. 9, pp. 1806–1819, Sep. 2011.
[13] H. Pirsiavash, D. Ramanan, and C. Fowlkes, "Globally-optimal greedy algorithms for tracking a variable number of objects," in *Proc. IEEE Conf. Comput. Vision Pattern Recog.*, 2011, pp. 1201–1208.
[14] M. D. Breitenstein, F. Reichlin, B. Leibe, E. Koller-Meier, and L. V. Gool, "Online multi-person tracking-by-detection from a single, uncalibrated camera," *IEEE Trans. Pattern Anal. Mach. Intell.*, vol. 33, no. 9, pp. 1820–1833, Sep. 2011.
[15] A. Andriyenko, K. Schindler, and S. Roth, "Discrete-continuous optimization for multi-target tracking," in *Proc. IEEE Conf. Comput. Vision Pattern Recog.*, 2012, pp. 1926–1933.
[16] A. Butt and R. T. Collins, "Multi-target tracking by Lagrangian relaxation to min-cost network flow," in *Proc. IEEE Conf. Comput. Vision Pattern Recog.*, 2013, pp. 1846–1853.
[17] A. V. Goldberg, "An efficient implementation of a scaling minimum-cost flow algorithm," *J. Algorithms*, vol. 22, pp. 1–29, 1992.
[18] B. Wang, G. Wang, K. L. Chan, and L. Wang, "Tracklet association with online target-specific metric learning," in *Proc. IEEE Conf. Comput. Vision Pattern Recog.*, 2014, pp. 1234–1241.
[19] C. H. Kuo and R. Nevatia, "How does person identity recognition help multi-person tracking?" in *Proc. IEEE Conf. Comput. Vision Pattern Recog.*, 2011, pp. 1217–1224.
[20] B. Yang and R. Nevatia, "Multi-target tracking by online learning of non-linear motion patterns and robust appearance models," in *Proc. IEEE Conf. Comput. Vision Pattern Recog.*, 2012, pp. 1918–1925.
[21] B. Yang and R. Nevatia, "Multi-target tracking by online learning a CRF model of appearance and motion patterns," *Int. J. Comput. Vision*, vol. 107, no. 2, pp. 203–217, 2014.
[22] P. Storms and F. Spieksma, "An LP-based algorithm for the data association problem in multitarget tracking," *Comput. Oper. Res.*, vol. 30, no. 7, pp. 1067–1085, 2003.
[23] H. Jiang, S. Fels, and J. Little, "A linear programming approach for multiple object tracking," in *Proc. IEEE Conf. Comput. Vision Pattern Recog.*, 2007, pp. 1–8.
[24] F. Fleuret, J. Berclaz, R. Lengagne, and P. Fua, "Multi-camera people tracking with a probabilistic occupancy map," *IEEE Trans. Pattern Anal. Mach. Intell.*, vol. 30, no. 2, pp. 267–282, Feb. 2008.
[25] B. Yang and R. Nevatia, "An online learned CRF model for multi-target tracking," in *Proc. IEEE Conf. Comput. Vision Pattern Recog.*, 2012, pp. 2034–2041.
[26] H. B. Shitrit, J. Berclaz, F. Fleuret, and P. Fua, "Multi-commodity network flow for tracking multiple people," *IEEE Trans. Pattern Anal. Mach. Intell.*, vol. 36, no. 8, pp. 1614–1627, Aug. 2014.
[27] W. Ge and R. T. Collins, "Multi-target data association by tracklets with unsupervised parameter estimation," in *Proc. Brit. Mach. Vision Conf.*, 2008, pp. 93.1–93.10.
[28] V. K. Singh, B. Wu, and R. Nevatia, "Pedestrian tracking by associating tracklets using detection residuals," in *Proc. IEEE Workshop Motion Video Comput.*, 2008, pp. 1–8.
[29] W. S. Zheng, S. Gong, and T. Xiang, "Re-identification by relative distance comparison," *IEEE Trans. Pattern Anal. Mach. Intell.*, vol. 35, no. 3, pp. 653–668, Mar. 2013.
[30] O. Camps, H. Li, M. C. Mazzaro, and M. Sznaier, "A Caratheodory-Fejer approach to robust multiframe tracking," in *Proc. IEEE Int. Conf. Comput. Vision*, 2003, pp. 1048–1055.
[31] T. Ding, M. Sznaier, and O. Camps, "Fast track matching and event detection," in *Proc. IEEE Conf. Comput. Vision Pattern Recog.*, 2008, pp. 1–8.
[32] B. Ho and R. Kalman, "Effective construction of linear, state-variable models from input/output functions," in *Regelungstechnik*, vol. 14, no. 10, pp. 545–548, 1966.
[33] M. Moonen, B. D. Moor, L. Vandenberghe, and J. Vandewalle, "On- and off-line identification of linear state space models," in *Int. J. Control*, vol. 49, no. 10, pp. 219–232, 1989.
[34] C. Dicle, O. Camps, and M. Sznaier, "The way they move: Tracking multiple targets with similar appearance," in *Proc. IEEE Int. Conf. Comput. Vision*, 2013, pp. 2304–2311.
[35] J. Ferryman and A. Shahrokni, "Pets2009: Dataset and challenge," in *Proc. IEEE 12th Int. Workshop Performance Evaluation Tracking Surveillance*, 2009, pp. 1–6.
[36] M. Andriluka, S. Roth, and B. Schiele, "People-tracking-by-detection and people-detection-by-tracking," in *Proc. IEEE Conf. Comput. Vision Pattern Recog.*, 2008, pp. 1–8.
[37] M. Andriluka, S. Roth, and B. Schiele, "Monocular 3D pose estimation and tracking by detection," in *Proc. IEEE Conf. Comput. Vision Pattern Recog.*, 2010, pp. 623–630.
[38] B. Benfold and I. Reid, "Stable multi-target tracking in real-time surveillance video," in *Proc. IEEE Conf. Comput. Vision Pattern Recog.*, 2011, pp. 3457–3464.
[39] A. Ess, K. S. B. Leibe, and L. van Gool, "Robust multiperson tracking from a mobile platform," *IEEE Trans. Pattern Anal. Mach. Intell.*, vol. 31, no. 10, pp. 1831–1846, Oct. 2009.
[40] K. Bernardin and R. Stiefelhagen, "Evaluating multiple object tracking performance: The CLEAR MOT metrics," *J. Image Video Process.*, vol. 2008, no. 1, pp. 1–10, 2008.
[41] A. Milan. (2012). Discrete-continuous optimization for multi-target tracking. [Online]. Available: http://www.gris.informatik.tu-darmstadt.de/ aandriye/dctracking.html
[42] (2015). Multiple object tracking benchmark. [Online]. Available: http://motchallenge.net/
[43] (2009). Robust multi-person tracking from mobile platforms. [Online]. Available: https://data.vision.ee.ethz.ch/cvl/aess/dataset/
[44] L. Leal-Taixe, A. Milan, I. Reid, S. Roth, and K. Schindler, "Motchallenge 2015: Towards a benchmark for multi-target tracking," *arXiv: 1504.01942 [cs]*, Apr. 2015, http://arxiv.org/abs/1504.01942

[45] A. Andriyenko and K. Schindler, "Multi-target tracking by continuous energy minimization," in *Proc. IEEE Conf. Comput. Vision Pattern Recog.*, 2011, pp. 1265–1272.
[46] J. F. Henriques, R. Caseiro, and J. Batista, "Globally optimal solution to multi-object tracking with merged measurements," in *Proc. IEEE Int. Conf. Comput. Vision*, 2011, pp. 2470–2477.
[47] M. Hofmann, M. Haag, and G. Rigoll, "Unified hierarchical multi-object tracking using global data association," in *Proc. IEEE Int. Workshop Performance Evaluation Tracking Surveillance*, 2013, pp. 22–28.
[48] M. Hofmann, D. Wolf, and G. Rigoll, "Hypergraphs for joint multi-view reconstruction and multi-object tracking," in *Proc. IEEE Conf. Comput. Vision Pattern Recog.*, 2013, pp. 3650–3657.
[49] H. Izadinia, I. Saleemi, W. Li, and M. Shah, "$(MP)^2T$: Multiple people multiple parts tracker," in *Proc. 12th Eur. Conf. Comput. Vision*, 2012, pp. 100–114.
[50] A. Milan, K. Schindler, and S. Roth, "Detection- and trajectory-level exclusion in multiple object tracking," in *Proc. IEEE Conf. Comput. Vision Pattern Recog.*, 2013, pp. 3682–3689.
[51] A. Milan, S. Roth, and K. Schindler, "Continuous energy minimization for multi-target tracking," *IEEE Trans. Pattern Anal. Mach. Intell.*, vol. 36, no. 1, pp. 58–72, Jan. 2014.
[52] A. R. Zamir, A. Dehghan, and M. Shah, "GMCP-tracker: Global multi-object tracking using generalized minimum clique graphs," in *Proc. 12th Eur. Conf. Comput. Vision*, 2012, pp. 343–356.
[53] Z. Wu, J. Zhang, and M. Betke, "Online motion agreement tracking," presented at the 24th British Machine Vision Conf., Bristol, United Kingdom, 2013.
[54] J. Yang, P. A. Vela, Z. Shi, and J. Teizer, "Probabilistic multiple people tracking through complex situations," in *Proc. Int. Workshop Performance Evaluation Tracking Surveillance*, 2009.
[55] H. Possegger, T. Mauthner, P. M. Roth, and H. Bischof, "Occlusion geodesics for online multi-object tracking," in *Proc. IEEE Conf. Comput. Vision Pattern Recog.*, 2014, pp. 79–86.
[56] S. Chen, A. Fern, and S. Todorovic, "Multi-object tracking via constrained sequential labeling," in *Proc. IEEE Conf. Comput. Vision Pattern Recog.*, 2014, pp. 1130–1137.
[57] L. Leal-Taixe, G. Pons-Moll, and B. Rosenhahn, "Everybody needs somebody: Modeling social and grouping behavior on a linear programming multiple people tracker," in *Proc. IEEE Int. Conf. Comput. Vision*, 2011, pp. 120–127.
[58] S. Pellegrini, A. Ess, K. Schindler, and L. V. Gool, "You'll never walk alone: Modeling social behavior for multi-target tracking," in *Proc. IEEE Int. Conf. Comput. Vision*, 2009, pp. 261–268.
[59] K. Yamaguchi, A. C. Berg, L. E. Ortiz, and T. L. Berg, "Who are you with and where are you going?" in *Proc. IEEE Conf. Comput. Vision Pattern Recog.*, 2011, pp. 1345–1352.
[60] L. Leal-Taixe, M. Fenzi, A. Kuznetsova, B. Rosenhahn, and S. Savarese, "Learning an image-based motion context for multiple people tracking," in *Proc. IEEE Conf. Comput. Vision Pattern Recog.*, 2014, pp. 3542–3549.
[61] S. H. Bae and K. J. Yoon, "Robust online multi-object tracking based on tracklet confidence and online discriminative appearance learning," in *Proc. IEEE Conf. Comput. Vision Pattern Recog.*, 2014, pp. 1218–1225.
[62] A. Geiger, M. Lauer, C. Wojek, C. Stiller, and R. Urtasun, "3D traffic scene understanding from movable platforms," in *IEEE Trans. Pattern Anal. Mach. Intell.*, vol. 36, no. 5, pp. 1012–1025, May 2014.
[63] J. Yoon, H. Yang, J. Lim, and K. Yoon, "Bayesian multi-object tracking using motion context from multiple objects," in *Proc. IEEE Winter Conf. Appl. Comput. Vision*, 2015, pp. 33–40.

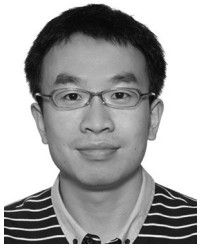

Bing Wang received the BE degree from Anhui University, China in 2011 and the ME degree from Nanyang Technological University, Singapore in 2012. He received the PhD degree from School of Electrical and Electronic Engineering, Nanyang Technological University, Singapore, in 2016. His research interests include computer vision, pattern recognition and machine learning. He is a student member of the IEEE.

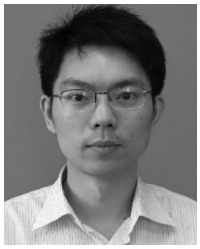

Gang Wang received the BS degree from the Harbin Institute of Technology, China, in 2005 and the PhD degree from the University of Illinois at Urbana-Champaign, Urbana. He is an assistant professor in electrical and electronic engineering at Nanyang Technological University. He is also a research scientist of the Advanced Digital Science Center. His research interests include computer vision and machine learning. He is a member of the IEEE.

Kap Luk Chan received the PhD degree in robot vision from the Imperial College of Science, Technology, and Medicine, University of London, London, United Kingdom, in 1991. He was an associate professor with the School of Electrical and Electronic Engineering, Nanyang Technological University, Singapore. He is currently the managing director of Tolendata Singapore R&D Centre and director of Technology in the Stratech Group Limited. His current research interests include image analysis and computer vision, and application of machine learning in computer vision, intelligent video surveillance. He is a member of the IEEE.

Li Wang received the BE degree from Southeast University, China, in 2006 and the ME degree from Shanghai Jiao Tong University, China, in 2009. He received the PhD degree from School of Electrical and Electronic Engineering, Nanyang Technological University, Singapore, in 2016. His research interests include computer vision and machine learning. He is a member of the IEEE.